

Isobar model analysis of $\pi^0\eta$ photoproduction on protons

A. Fix,^{1,*} V.L. Kashevarov,^{2,3,†} A. Lee,¹ and M. Ostrick²

¹*Tomsk Polytechnic University, Tomsk, Russia*

²*Institut für Kernphysik, Johannes Gutenberg-Universität Mainz, Mainz*

³*Lebedev Physical Institute, Moscow, Russia*

(Dated: today)

Photoproduction of $\pi^0\eta$ on protons in the energy range from threshold to 1.4 GeV is discussed. The data for representative angular distributions recently obtained at MAMI C are analyzed using an isobar model. The isobars considered are $\Delta(1232)$ and $S_{11}(1535)$ for π^0p and ηp states, respectively. In accordance with the results of earlier works the main features of the reaction are explained through the dominance of the D_{33} wave with a relatively small admixture of positive parity resonances. Comparison with recent experimental results for the photon beam asymmetry is carried out.

PACS numbers: 25.20.Lj, 13.60.Le, 14.20.Gk

I. INTRODUCTION

Several important features of $\pi^0\eta$ photoproduction on protons were explained in earlier papers [1–4], where different versions of an isobar model were used as a theoretical basis. According to the experimental results of [3–5] the cross section for $\gamma p \rightarrow \pi^0\eta p$ exhibits quite a rapid rise at low energies and reaches its characteristic value $\sigma \approx 3.5 \mu\text{b}$ at $E_\gamma = 1.4 \text{ GeV}$, about 0.5 GeV above threshold. Such a behavior might indicate that the cross section is mainly governed by the increasing phase space so that it is dominated by s -waves. As has been noted in [1, 6] the Born terms seem to be insignificant and the reaction is expected to proceed via formation of baryon resonances decaying into $\pi\eta N$.

Within an isobar model, production of two mesons may conveniently be described in terms of intermediate quasi-two-body states, the isobars. These states naturally appear if the attractive two-body interaction between the final particles lead to narrow resonances. In the case of the $\pi\eta N$ state the πN and ηN isobars are identified with the $\Delta(1232)$ and $S_{11}(1535)$ which are well known to dominate πN and ηN scattering. In such a picture the observed growth of the total cross section would point to the existence of baryon resonances, belonging to the third resonance region, which may decay into s -wave $\eta\Delta$ or πS_{11} configurations. One can easily show that only in the $D_{33}(P_{31})$ state the $\eta\Delta$ (πS_{11}) system can be produced in the relative s -wave.

The model for $\gamma N \rightarrow \pi^0\eta N$, with the resonance $D_{33}(1700)$ dominating the amplitude, has been developed in ref. [1], where $\pi^0\eta$ and $\pi^0 K^0$ photoproduction were studied within a coupled channel approach. The authors used the $D_{33} \rightarrow \eta\Delta$ decay, treated on a tree level, as a main driving mechanism. The crucial importance of D_{33} in this calculation is ultimately a consequence of quite a large (complex) coupling constant $g_{\eta\Delta}$ whose

value $g_{\eta\Delta} = 1.7 - 1.4i$ was taken from [7]. The production of the πS_{11} state is calculated microscopically as a series of interactions $\eta\Delta \rightarrow (\pi\eta N, \pi K\Lambda, \pi K\Sigma) \rightarrow \pi S_{11}$ taken up to the first order in the two-body t -matrices for ηN and $K\Lambda$ ($K\Sigma$) scattering.

On the experimental side, recent studies [3, 4, 8] have also implied that the resonance $D_{33}(1700)$ plays a crucial role in $\pi^0\eta$ photoproduction. In ref. [3] the data for $\gamma p \rightarrow \pi^0\eta p$ were explained using the PWA method [9] which gave definite quantitative conclusions about contributions of different N - and Δ -like resonances. In particular, the authors reported that at higher energies ($W > 1.8 \text{ GeV}$) the D_{33} wave remains important and is presumably populated by the $D_{33}(1940)$ resonance.

In ref. [4], in addition to the basic cross section, the linear beam asymmetry Σ was measured. In common with the results of [3] the authors of [4] emphasized the dominance of the $D_{33}(1700)$. The importance of the $\eta\Delta$ configuration is indicated by the pronounced peak in the π^0p mass spectra around the Δ mass. The data for the Σ -asymmetry are in general agreement with the predictions of the model [1]. The $D_{33}(1700)$ dominance is deduced from the fact that without this resonance one obtains strong qualitative disagreement with the measured asymmetry.

A remarkable feature of the data reported in ref. [4] is that the πS_{11} configuration appears to not be as pronounced as it may follow from the theoretical calculation of ref. [1]. The case in point is that the apparent shifting of the π^0p peak predicted by the model [1] is not evident from the experimental results. Instead of this, as is shown in [4], the simple model containing only $\eta\Delta$ decay accounts for the data much better than the sophisticated approach including πS_{11} formation. On the other hand, trivial assumption that the role of πS_{11} configuration in $\gamma p \rightarrow \pi^0\eta p$ is negligible may lead to misinterpretation of the data. It is clear that the $S_{11}(1535)$ resonance should, in any case, be present on the Dalitz plot due to the ηN final state interaction. The reason for its 'disappearance' may lie in the fact that the ηN scattering cross section does not exhibit a true resonance behavior due to the closeness of the resonance mass to the

*Electronic address: fix@mph.phtd.tpu.ru

†Electronic address: kashev@kph.uni-mainz.de

ηN threshold. Furthermore, the presence of an intensive $D_{33} \rightarrow \eta \Delta$ decay makes it difficult to estimate quantitatively the role of the πS_{11} channel. These observations suggest that studying πN or ηN invariant mass distributions does not enable us to clarify the separation of the events related to πS_{11} formation. In this connection, it is desirable to have methods allowing identification of πS_{11} without recourse to the ηN invariant mass distribution.

The crucial role of the D_{33} configuration in $\pi^0 \eta$ photoproduction is a very important result by itself. It implies that, apart from the (γ, π^0) and (γ, η) reactions determined respectively by the Δ and S_{11} formation, we have another process, $(\gamma, \pi^0 \eta)$, whose amplitude in a wide energy range is mainly governed by a single dynamical mechanism, the excitation of the D_{33} wave, in particular the $D_{33}(1700)$ state. Clearly, this feature provides an effective method to study the properties of this resonance. However, in contrast to single π^0 or η photoproduction, here we face the technical problems associated with three-body kinematics, where the particle energies and angles are distributed continuously. It therefore becomes difficult to perform a general multipole analysis, primarily since there is a multitude of ways to couple angular momenta of particles to the total angular momentum.

Important steps on the road to a systematic study of the partial wave structure of $\pi^0 \eta$ photoproduction were made in ref. [6], where the authors presented a phenomenological model for $\gamma N \rightarrow \pi^0 \eta N$ and discussed the angular distributions of final particles. Although, in general, unpolarized measurements are not sufficient to distinguish between all partial waves, assuming that only one of these waves is important, it is possible to reach a rather definite conclusion about the corresponding quantum numbers. The analysis permits the identification of the quantum numbers of the dominant resonance states simply by analysing the shape of the measured angular dependencies, in which the states with different spin-parities exhibit their own signatures. It is also emphasized in [6] that some of the observables depend weakly on the model parameters. This fact makes such a method especially useful.

The formalism developed in ref. [6] was then applied to the analyses of the data recently obtained at MAMI C [8]. As a main subject, the authors of [8] studied the angular distributions of particles in $\gamma p \rightarrow \pi^0 \eta p$. This approach was shown to be very effective as a tool to study the properties of the $D_{33}(1700)$ resonance. In particular, the ratio of πS_{11} to $\eta \Delta$ decay widths, which, as pointed out above, is difficult to extract from the invariant mass distribution, was deduced from the data with appreciated accuracy.

Here we continue the analysis of the reaction $\gamma N \rightarrow \pi^0 \eta N$ using the isobar model which was partially described in refs. [6] and [8]. The paper is organized as follows. In the next section we briefly outline the formalism, and summarize some results, of ref. [6] which provides a framework for the calculation to follow. Then in Sect. III we present our results where the main emphasis

is put on the angular distributions of the final particles. In Sect. III B we consider in some detail the photon asymmetry Σ for $\gamma p \rightarrow \pi^0 \eta p$ and discuss the main properties of this observable. In Sec. IV we close with a brief summary and an outlook.

II. THEORETICAL BASIS

We consider the reaction

$$\begin{aligned} \gamma(\omega_\gamma, \vec{k}) + N_i(E_i, -\vec{k}) \\ \rightarrow \pi^0(\omega_\pi, \vec{q}_\pi) + \eta(\omega_\eta, \vec{q}_\eta) + N_f(E_f, \vec{p}_f) \end{aligned} \quad (1)$$

in the overall center-of-mass system. The corresponding energies and three-momenta of the particles are given in the parentheses. Furthermore, throughout the paper we use the following notations for kinematic variables:

| | |
|---|---|
| E_γ | photon lab energy, |
| W | total c.m. energy, |
| $\omega_\alpha, \quad \alpha = \pi N, \eta N$ | invariant energy of the two-particle subsystem α , |
| $\Omega_i = (\Theta_i, \Phi_i), \quad i = \pi, \eta$ | solid angle of the momentum \vec{q}_i in the overall c.m. frame, |
| $\omega_i^*, \vec{q}_i^*, \quad i = \pi, \eta$ | energy and three-momentum of the i -th particle in the iN c.m. frame, |
| $\Omega_i^{K(H)} = (\theta_i^{K(H)}, \phi_i^{K(H)}), \quad i = \pi, \eta$ | solid angle of the momentum \vec{q}_i^* , related to the $K(H)$ system. |

The meaning of K and H systems is explained by Fig. 2 (see also text after eq. (8)).

A theoretical basis of our calculation is presented in ref. [6] and partially in ref. [8]. We assume that the $\pi \eta$ system does not resonate over the energy region in question. The reaction amplitude is divided into the Born and the resonance part,

$$t_{m_f \lambda} = t_{m_f \lambda}^B + t_{m_f \lambda}^R, \quad (2)$$

and is visualized by means of the diagrams in Fig. 1. The indices $m_f = \pm 1/2$ and $\lambda = \pm 1/2, \pm 3/2$ denote the z -projection of the final nucleon spin and the initial state helicity, respectively. The Born sector is formed by the diagrams (a)-(f). As already noted, its role in the channel $\pi^0 \eta p$ turns out to be insignificant.

According to the isobar model concept, the resonance part of the amplitude may be superposed in the usual

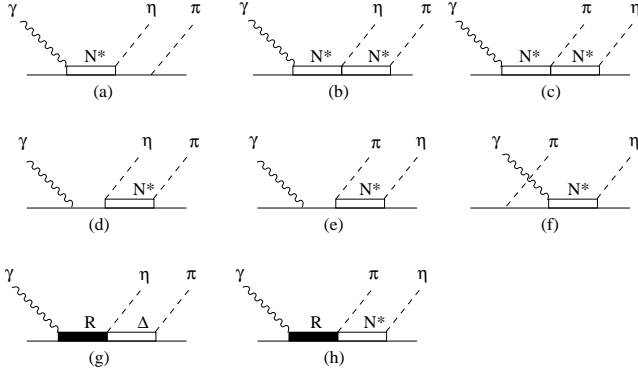


FIG. 1: Diagrams representing the amplitude for the $\gamma N \rightarrow \pi \eta N$ reaction in a simple isobar model. The notations Δ and N^* are used for the resonances $\Delta(1232)$ and $S_{11}(1535)$.

fashion, as a sum of two terms ¹

$$t_{m_f \lambda}^R = t_{m_f \lambda}^{(\eta \Delta)} + t_{m_f \lambda}^{(\pi N^*)} \quad (3)$$

corresponding to the diagrams (g) and (h) in Fig. 1. Each term in eq. (3) has the form

$$t_{m_f \lambda}^{(\alpha)}(W, \vec{q}_\pi, \vec{q}_\eta, \vec{p}_f) = \sum_{R(J^\pi; T)} C_T A_\lambda^R(W) G_R(W) \times f_{m_f \lambda}^{R(\alpha)}(W, \vec{q}_\pi, \vec{q}_\eta, \vec{p}_f), \quad \alpha = \eta \Delta, \pi N^*, \quad (4)$$

where the summation is over the resonance states determined by their spin-parity J^π and isospin T . The latter is incorporated through the factor C_T . Since the η -meson has isospin zero, this factor is the same for both the $\eta \Delta$ and πN^* channels. In our case, where only the states with $T = 3/2$ are assumed to contribute, C_T is $2/3$.

The functions $A_\lambda^R(W)$ are the helicity amplitudes for $\gamma p \rightarrow R$. Their energy dependence was parametrized in the simple form

$$A_\lambda^R(W) = A_\lambda^R(M_R) \left(\frac{\omega_\gamma}{\omega_\gamma^R} \right)^{n_\lambda}, \quad (5)$$

where M_R is the resonance mass and ω_γ^R is the c.m. photon energy, calculated at the resonance position. For the dominant resonance, $D_{33}(1700)$, the exponent $n_{1/2}$ was set equal to 1, whereas the function $A_{3/2}^{D_{33}}(W)$ was fitted to the data separately in each energy bin in Fig. 5. For the other resonances we used $n_\lambda = 0$.

The factors $G_R(W)$ stand for the resonance propagators for which we use the nonrelativistic Breit-Wigner form

$$G_R(W) = \frac{1}{W - M_R + \frac{i}{2} \Gamma_{tot}^R(W)}. \quad (6)$$

¹ In the expressions to follow the resonance $S_{11}(1535)$ is denoted by N^* .

In eq. (4), the functions $f_{m_f \lambda}^{R(\alpha)}$, $\alpha = \eta \Delta, \pi N^*$, describe the decay of the resonance R into $\pi \eta N$ via intermediate formation of $\eta \Delta$ and πN^* states.

We take the Z -axis of the overall c.m. frame along the photon momentum \vec{k} . The OXZ plane is spanned by the momenta \vec{k} and \vec{q}_η (see Fig. 2). To fix the final state kinematics we choose as independent variables the particle momenta associated with the partition $\eta + (\pi N)$, the solid angle of the η momentum $\Omega_\eta = (\Theta_\eta, \Phi_\eta = 0)$, the invariant energy $\omega_{\pi N}$ of πN subsystem, and the solid angle of the momentum \vec{q}_π^* in the πN rest frame.

For the data analysis, two types of coordinate systems $O'x'y'z'$, related to the πN c.m. frame, are used. In the first one, the canonical (K) system (Fig. 2(a)), the axes are chosen parallel to those in the main c.m. frame $OXYZ$ fixed in space. In the helicity (H) system (Fig. 2(b)) the z' -axis is taken to be along $\vec{q}_\pi + \vec{p}_f = -\vec{q}_\eta$. For a single event the systems are connected via appropriate rotation by the angle $\pi - \Theta_\eta$ around the y' -axis. After integrating over Θ_η is carried out this equivalence does not hold, and in this sense the distributions $W(\Omega_i^K)$ and $W(\Omega_i^H)$, $i = \pi, \eta$ are independent. The values related to the K and H frames are further denoted by the indices K and H respectively.

In the K system, the pion momentum, \vec{q}_π^* , is related to the pion momentum \vec{q}_π in the overall c.m. frame via the Lorentz boost along the vector $-\vec{q}_\eta$, giving

$$\vec{q}_\pi = \vec{q}_\pi^* + X_\pi \vec{q}_\eta, \quad X_\pi = -\frac{\omega_\pi^* + \omega_\pi}{\omega_{\pi N} + W - \omega_\eta}. \quad (7)$$

In Sect. III B we also use the partition $\pi + (\eta N)$, taking as independent kinematical variables the solid angle $\Omega_\pi = (\Theta_\pi, \Phi_\pi = 0)$, the invariant energy $\omega_{\eta N}$, and the spherical angles of the η momentum in the ηN c.m. frame. In this case the reaction plane is spanned by the vectors \vec{k} and \vec{q}_π . The relation between the momentum of the η meson is similar to that in (7):

$$\vec{q}_\eta = \vec{q}_\eta^* + X_\eta \vec{q}_\pi, \quad X_\eta = -\frac{\omega_\eta^* + \omega_\eta}{\omega_{\eta N} + W - \omega_\pi}. \quad (8)$$

We adhere to the non-relativistic concept of angular momentum and do not include, for instance, effects of spin transformation caused by the Lorentz boost. Then, in the coordinate system chosen, the angular dependence of the amplitudes (4) may be decomposed by means of spherical functions. In the K system, associated with the partition $\eta + (\pi N)$ (Fig. 2) we will have

$$f_{m_f \lambda}^{R(\eta \Delta)K} = F^{R(\eta \Delta)}(\omega_{\pi N}) \sum_m C_{1m \frac{1}{2}m_f}^{\frac{3}{2}M_\Delta} \times C_{L_\eta M_\eta \frac{3}{2}M_\Delta}^{J\lambda} Y_{1m}(\Omega_\pi^K) d_{M_\eta 0}^{L_\eta}(\Theta_\eta), \quad (9)$$

$$f_{m_f \lambda}^{R(\pi N^*)K} = F^{R(\pi N^*)}(\omega_{\eta N}) C_{L_\pi M_\pi \frac{1}{2}m_f}^{J\lambda} \sum_{l=0}^{L_\pi} A_l \times \sum_m C_{L_\pi - l M_\pi - m}^{L_\pi M_\pi} Y_{lm}(\Omega_\pi^K) d_{M_\pi - m 0}^{L_\pi - l}(\Theta_\eta). \quad (10)$$

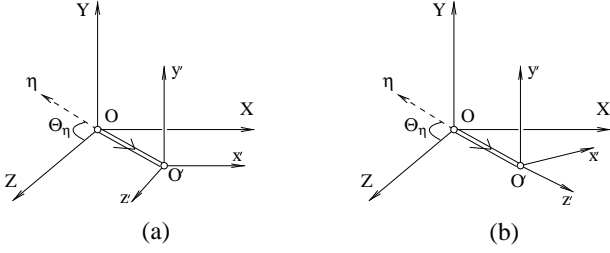


FIG. 2: The coordinate systems ($x'y'z'$) used for the analysis of angular distributions of pions in the πp rest frame. In the canonical system (K system) the z' axis is taken parallel to the beam direction, whereas in the helicity system (H system) it is aligned along the total πp momentum. In both systems, the x' axis is in the reaction plane and the y' axis is chosen as $\hat{y}' = (\vec{p}_\eta \times \vec{k}_\gamma) / |\vec{p}_\eta \times \vec{k}_\gamma|$.

Here, $C_{j_1 m_1 j_2 m_2}^{j_3 m_3}$ are the usual Clebsch-Gordan coefficients for the coupling $\vec{j}_1 + \vec{j}_2 = \vec{j}_3$. The coefficients A_l , determined as

$$A_l = \left(\frac{X_\pi q_\eta}{q_\pi^*} \right)^l \sqrt{\frac{(2L_\pi - 1)(2L_\pi)!}{(2l - 1)(2L_\pi - 2l)!(2l)!}}, \quad (11)$$

stem from the expansion of the function $Y_{L_\pi M_\pi}(\Omega_\pi)$ over the products of the spherical functions depending on Ω_π^K and Ω_η .

The corresponding expressions for $f_{m_f \lambda}^{R(\alpha)K}$ can easily be obtained from eqs. (9) and (10) via rotation of $Y_{lm}(\Omega_\pi^K)$ by the angle Θ_η around the Y axis.

The coefficients $F^{R(\alpha)}(\omega)$, $\alpha = \eta\Delta, \pi N^*$ are parametrized in terms of coupling constants

$$F^{R(\eta\Delta)}(\omega_{\pi N}) = \frac{f_{R\eta\Delta} f_{\Delta\pi N}}{m_\pi^{L_\eta+1}} G_\Delta(\omega_{\pi N}) q_\eta^{L_\eta} q_\pi^*, \quad (12)$$

$$F^{R(\pi N^*)}(\omega_{\eta N}) = \frac{f_{R\pi N^*} f_{N^*\eta N}}{m_\pi^{L_\pi}} G_{N^*}(\omega_{\eta N}) q_\pi^{*L_\pi}, \quad (13)$$

where G_Δ and G_{N^*} are the Δ and N^* isobar propagators.

Unlike ref. [1] here we use a phenomenological rather than a dynamical approach to describe the transition to πN^* . Namely, the vertex $R \rightarrow \pi N^*$ appearing in the diagram (h) in Fig. 1 was parametrized in the form of an ordinary resonance decay $R \rightarrow \pi N^*$ fixed by the constant $f_{R\pi N^*}$ (see eq. (13)). In contrast, in ref. [1] only the $\eta\Delta$ decay is treated as a 'primary process' whereas πN^* is generated during the ηp final state interaction. As noted in [6], we expect our approximation to be reasonable at least around the resonance maximum.

The angular distributions are analysed in terms of the functions $W(\theta)$ and $W(\phi)$ which are differential cross sec-

TABLE I: Angular momenta associated with a decay of the resonance $R(J^\pi)$ into the channels $\eta\Delta$ (denoted by L_η) and πN^* (L_π).

| $J^\pi(L_{2T2J})$ | L_η | L_π |
|-------------------------|----------|---------|
| $\frac{1}{2}^-(S_{31})$ | 2 | 1 |
| $\frac{1}{2}^+(P_{31})$ | 1 | 0 |
| $\frac{3}{2}^-(D_{33})$ | 0, 2 | 1 |
| $\frac{3}{2}^+(P_{33})$ | 1, 3 | 2 |
| $\frac{5}{2}^-(D_{35})$ | 2, 4 | 3 |
| $\frac{5}{2}^+(F_{35})$ | 1, 3 | 2 |

tions normalized to unity. For instance,

$$W(\theta_\pi^K) = \frac{1}{\sigma} \int_0^{2\pi} \frac{d\sigma}{d\Omega_\pi^K} d\phi_\pi^K, \quad (14)$$

$$W(\phi_\pi^K) = \frac{1}{\sigma} \int_0^\pi \frac{d\sigma}{d\Omega_\pi^K} \sin \theta_\pi^K d\theta_\pi^K, \quad (15)$$

with σ standing for the total cross section.

To effectively include the total cross section into the fitting procedure we use the products $\bar{\sigma}W(\theta_\pi^{K(H)})$ and $\bar{\sigma}W(\phi_\pi^{K(H)})$, where $\bar{\sigma}$ is the total cross section, averaged over the corresponding energy bin.

The adjustable parameters are collected in Table II. Since the resonance amplitudes are proportional to the product of the electromagnetic and hadronic couplings, the amplitudes A_λ and the ratios $\beta_\alpha = \Gamma_{\pi\eta N}^{(\alpha)} / \Gamma_{tot}^R$, $\alpha = \eta\Delta, \pi N^*$, cannot be well determined individually. For this reason, we use the quantity $\sqrt{\beta_{\eta\Delta}} A_{1/2}$ together with the ratio of the helicity amplitudes $A_{3/2}$ and $A_{1/2}$, and the ratio r of $R \rightarrow \pi N^*$ and $R \rightarrow \eta\Delta$ branchings.

We note that our fitting procedure did not include varying the total widths. The reason lies in the closeness of the resonances, especially $D_{33}(1700)$, to the $\pi\eta$ production threshold. As a result, the set of angular distributions alone does not impose sufficiently stringent constraints on the values of the resonance widths, and to some extent, on their masses. In this respect, we fix the widths, taking their values from the PDG compilation [10] or from the references cited there (the width of $D_{33}(1700)$ was taken from the recent analysis of [11] and that of $P_{31}(1750)$ from ref. [12]). For the same reason, the masses of the well known resonances, rated by four or three stars, were varied around their values given by PDG [10].

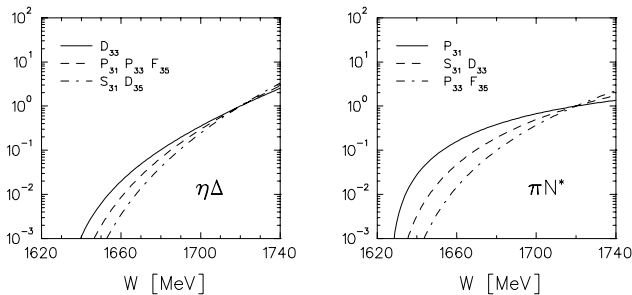


FIG. 3: Powers of $\eta\Delta$ and πN^* relative momenta averaged over the isobar distribution as functions of the total c.m. energy. As indicated in the legend, the curves determine energy dependence of partial decay widths of the corresponding resonances (see eqs. (16) and (17)). As noted in text, for $R \rightarrow \eta\Delta$ decay only the lowest value of the orbital momenta L_η is considered.

The orbital angular momenta L_η and L_π related to the $\eta\Delta$ and πN^* decays of the resonances are listed in Table I. As discussed in Sect. III A, in the $D_{33}(1700) \rightarrow \eta\Delta$ decay we included both s - and d -waves. As for other resonance states, for the sake of simplicity, we take only the lowest of the two possible values of L_η (see Table I).

III. DISCUSSION OF THE RESULTS

The general properties of the measured angular distributions and energy spectra were considered in ref. [8]. To interpret the data, the authors of ref. [8] used the single resonance model. It was assumed that there is one resonance (or, in general case, one partial wave) dominating the amplitude in a wide energy region. Following this concept they retain only one term in the sum (4) to roughly reproduce the main features of the observed angular distributions and thus to reach a tentative conclusion about the quantum numbers of this dominant resonance.

The results obtained in ref. [8] are now used as a starting point for a more refined analysis. Namely, having established the appropriate magnitude of the dominant partial wave, we successively add other waves in order to reproduce the structural details of the measured quantities. Thereupon we calculate the angular distributions measured in ref. [3], as well as the photon beam asymmetry presented in [4] and [13], and compare our results with the data.

A. Angular distributions

Before dealing with the results of our fit, it is instructive to qualitatively discuss the role of different partial waves in the angular distributions obtained in the experiment. Firstly, we consider the near-threshold region

where the energy is not high enough to produce isobars in higher angular momentum states, so that spin-parity selection rules may be used at least for qualitative estimations. In essence, the question is related to the energy dependence of the partial decay widths for $R \rightarrow \alpha \rightarrow \pi\eta N$, $\alpha = \eta\Delta$, πN^* , which in turn are determined by the appropriate powers of the $\eta\Delta$ and πN^* relative momenta averaged over the isobar distribution in the available phase space:

$$\langle q_\eta^{2L_\eta+1} \rangle(W) = \frac{1}{2\pi} \int_{M_N+m_\pi}^{W-m_\eta} q_\eta^{2L_\eta+1}(W, \omega) \frac{\Gamma_\Delta(\omega)}{(\omega - M_\Delta)^2 + \Gamma_\Delta(\omega)^2/4} \omega d\omega, \quad (16)$$

$$\langle q_\pi^{2L_\pi+1} \rangle(W) = \frac{1}{2\pi} \int_{M_N+m_\eta}^{W-m_\pi} q_\pi^{2L_\pi+1}(W, \omega) \frac{\Gamma_{N^*}(\omega)}{(\omega - M_{N^*})^2 + \Gamma_{N^*}(\omega)^2/4} \omega d\omega. \quad (17)$$

The particle momenta appearing in eq. (16) and (17) are determined by the usual kinematic formula

$$q_i(W, \omega) = \frac{\lambda^{1/2}(W, \omega, m_i)}{2W}, \quad i = \pi, \eta \quad (18)$$

with λ standing for the triangle function $\lambda(x, y, z) = (x - y - z)^2 - 4yz$.

In Fig. 3 we present the ratio $\langle q_i^{2L_i+1} \rangle(W) / \langle q_i^{2L_i+1} \rangle(M)$, $i = \pi, \eta$, calculated for $M = 1.72$ GeV with typical isobar masses and widths:

$$M_\Delta = 1232 \text{ MeV}, \quad \Gamma_\Delta(M_\Delta) = 120 \text{ MeV},$$

$$M_{N^*} = 1535 \text{ MeV}, \quad \Gamma_{N^*}(M_{N^*}) = 150 \text{ MeV},$$

$$\Gamma_{N^* \eta N}(M_{N^*}) = 45\% \Gamma_{N^*}(M_{N^*}).$$

As might be expected, in each individual channel, $\eta\Delta$ or πN^* , the energy dependence of the partial cross sections exhibits the typical threshold behavior $\sigma_{L_i} \sim \langle q^{2L_i+1} \rangle$, $i = \pi, \eta$. This simple relation, however, is slightly violated in the real situation when both configurations, $\eta\Delta$ and πN^* , are included. Firstly, because of the different parities of Δ and N^* the values L_η and L_π , entering the same partial wave J^π , always differ by 1. Secondly, the nominal thresholds corresponding to the production of stable Δ and N^* are $E_\gamma = 1.22$ and 1.01 GeV, respectively, for $\eta\Delta$ and πN^* channels. As a result, the $\eta\Delta$ channel is effectively opened at energies about 200 MeV higher than those associated with πN^* production. Furthermore, the smaller mass of the pion, in comparison to the η , leads to the availability of a larger phase space for the πN^* configuration already at rather low energies. By referring to Fig. 3 it may be seen that in the $\eta\Delta$ channel the D_{33} state exhibits the largest rate of growth. The

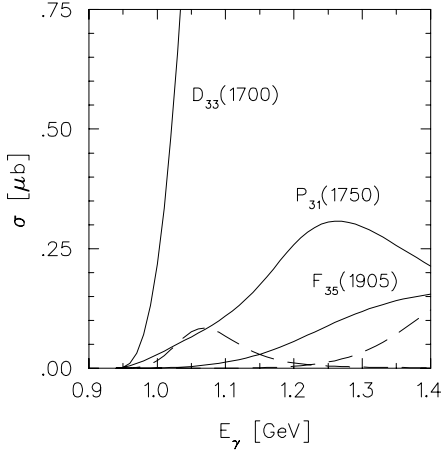


FIG. 4: Estimate of resonance contributions to $\gamma p \rightarrow \pi^0 \eta p$ according to formula (3). Presented are the resonances which were examined in the quark model analysis of ref. [14] as the baryons decaying into the $\eta\Delta$ channel. The dashed lines show the contribution of $P_{33}(1600)$ and $P_{33}(1920)$. For the electromagnetic and hadronic decay widths the values from the PDG compilation [10] are taken. For the partial widths $\Gamma_{\pi\eta N}$ the same relation $\Gamma_{\pi\eta N} = 0.1 \Gamma_{tot}$ for each resonance is used.

next most important waves are P_{31} and P_{33} , producing the $\eta\Delta$ system in the relative $L_\eta = 1$ state. Furthermore, the P_{31} , leading to the s -wave in the πN^* mode, may kinematically be the most favorable wave close to the threshold.

Some Δ resonances, which may be coupled with the $\eta\Delta$ state, were calculated within the constituent quark model of ref. [14]. A rough estimation of their contribution can be made by taking the corresponding parameters from the Particle Data Tables [10]. Neglecting background and using unitarity one arrives at the sum over the resonance states R

$$\sigma(W) \approx \sum_R \sigma^R(W), \quad (19)$$

with the partial cross section reading

$$\sigma^R(W) = \frac{\pi}{\omega_\gamma^2} (2J_R + 1) \frac{\Gamma_{\pi\eta N}^R(W) \Gamma_{\gamma N}^R(W)}{(W - M_R)^2 + \Gamma_{tot}^2(W)/4}. \quad (20)$$

The cross section predicted by formula (19) is plotted in Fig. 4 together with the contributions of the individual resonances. For the partial decay widths we used the common relation $\Gamma_{\pi\eta N}(M) = 0.1 \Gamma_{tot}(M)$ for all states. Although this estimate is very rough because of the uncertainties in the partial widths $\Gamma_{\pi\eta N}$, one can expect that the $P_{33}(1600)$ resonance already mentioned can really be visible near the threshold, whereas the $P_{31}(1750)$ and $F_{35}(1905)$ may come into play at higher energies.

Since we expect the D_{33} to dominate, it is useful to have an analytic expression for the cross section containing only D_{33} . Retaining in the sum (4) the term with

$J^\pi = 3/2^-$, and using in eqs. (9) and (10) $L_\eta = 0$ (for the moment we omit the d -wave in the $D_{33} \rightarrow \eta\Delta$ decay) and $L_\pi = 1$ from Table I, we obtain in the H system

$$\begin{aligned} \frac{d\sigma}{d\omega_{\pi N} d\Omega_\pi^H d\cos\Theta_\eta} \sim & \frac{2}{3} \left(A_{1/2}^2 + A_{3/2}^2 \right) \left(|c_1|^2 + |c_2|^2 + 2\text{Re}(\bar{c}_1 c_2) \cos\theta_\pi^H \right) \\ & + \frac{1}{2} \left(A_{1/2}^2 - A_{3/2}^2 \right) \left[\frac{2}{3} (1 - 3\cos^2\Theta_\eta) \right. \\ & \times \left(|c_1|^2 + |c_2|^2 + 2\text{Re}(\bar{c}_1 c_2) \cos\theta_\pi^H - \frac{3}{2} |c_1|^2 \sin^2\theta_\pi^H \right) \\ & + \left(2|c_1|^2 \cos\theta_\pi^H + \text{Re}(\bar{c}_1 c_2) \right) \sin 2\Theta_\eta \sin\theta_\pi^H \cos\phi_\pi^H \\ & \left. - |c_1|^2 \sin^2\Theta_\eta \sin^2\theta_\pi^H \cos 2\phi_\pi^H \right], \end{aligned} \quad (21)$$

where we omitted unessential kinematic factors. The coefficients c_1 and c_2 in (21) depend only on $\cos\theta_\pi^H$ and $\omega_{\pi N}$, and are independent of Θ_η and ϕ_π^H . In terms of the functions $F^{D_{33}(\alpha)}$ (12) and (13) they read

$$c_1 = \left(F^{D_{33}(\eta\Delta)} + F^{D_{33}(\pi N^*)} \right) q_\pi^*, \quad (22)$$

$$c_2 = F^{D_{33}(\pi N^*)} X_\pi q_\eta. \quad (23)$$

The factor X_π in eq. (23) comes from the Lorentz transformation to the πN rest frame $\vec{q}_\pi \rightarrow \vec{q}_\pi^*$ (see eq. (7)). The angular distribution $W(\Omega_\pi^H)$ can easily be obtained from (21) via appropriate integration. Since c_1 and c_2 are independent of Θ_η , the integration over $\cos\Theta_\eta$ is trivial and we arrive at

$$W(\theta_\pi^H) = A + B \cos\theta_\pi^H, \quad (24)$$

with

$$\begin{aligned} A &= \frac{1}{N} \int (|c_1|^2 + |c_2|^2) d\omega_{\pi N}, \\ B &= \frac{2}{N} \int \text{Re}(\bar{c}_1 c_2) d\omega_{\pi N}, \end{aligned} \quad (25)$$

where the normalization factor reads

$$\begin{aligned} N &= \int (|c_1|^2 + |c_2|^2 \\ &\quad + 2\text{Re}(\bar{c}_1 c_2) \cos\theta_\pi^H) d\omega_{\pi N} d\cos\theta_\pi^H. \end{aligned} \quad (26)$$

It is worth mentioning that the quantities A and B in eq. (24) are still functions of $\cos\theta_\pi^H$.

The distribution over the azimuthal angle ϕ_π^H , obtained via integration of the cross section (21) over $\cos\Theta_\eta$, $\cos\theta_\pi^H$, and $\omega_{\pi N}$, has the form

$$W(\phi_\pi^H) = \frac{1}{2\pi} \left(1 + \frac{1-a}{1+a} C \cos 2\phi_\pi^H \right). \quad (27)$$

The coefficient C is independent of ϕ_π^H and reads

$$C = \frac{1}{N} \int |c_1|^2 \sin^2\theta_\pi^H d\omega_{\pi N} d\cos\theta_\pi^H. \quad (28)$$

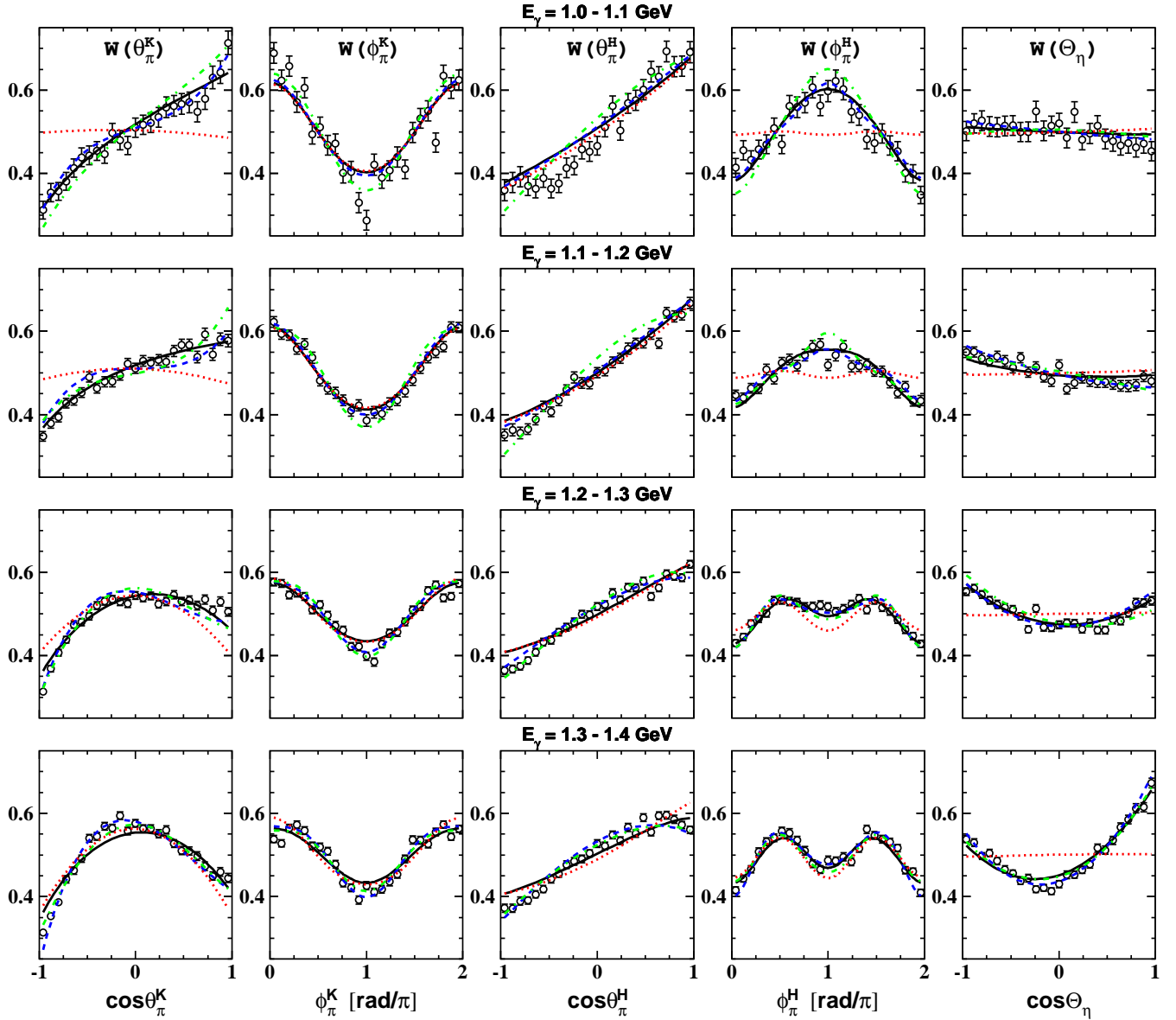


FIG. 5: Angular distributions of pions calculated in the canonical and helicity coordinate systems (the first four columns) and angular distribution of η mesons in the overall γp c.m. frame (the fifth column). The data are taken from [8]. The curves are our isobar model calculation corresponding to the solutions presented in Table II: solution I (solid), solution II (dashed), solution III (dash-dotted). The dotted curve is obtained within the single D_{33} model, including both $D_{33}(1700)$ and $D_{33}(1940)$ resonances. In the last case the parameters of both resonances were taken from the solution I.

The parameter a is determined by the ratio of the D_{33} helicity amplitudes as

$$a(W) = \left(\frac{A_{3/2}^{D_{33}}(W)}{A_{1/2}^{D_{33}}(W)} \right)^2. \quad (29)$$

Several conclusions important for understanding the experimental data presented below can be drawn. Firstly, as is found in ref. [8], the distribution $W(\theta_\pi^H)$ is rather sensitive to the relative contribution of the πN^* channel

to the $D_{33}(1700)$ decay. Quantitatively this sensitivity was discussed in [8] in terms of the parameter

$$r = \frac{\Gamma_{D_{33} \rightarrow \pi \eta N}^{(\pi N^*)}}{\Gamma_{D_{33} \rightarrow \pi \eta N}^{(\eta \Delta)}}, \quad (30)$$

where $\Gamma_{D_{33} \rightarrow \pi \eta N}^{(\alpha)}$, $\alpha = \eta \Delta, \pi N^*$, stands for the corresponding partial decay width.

From (23) and (24) one sees that if the contribution of πN^* vanishes, $W(\theta_\pi^H)$ becomes isotropic ($B = 0$). The

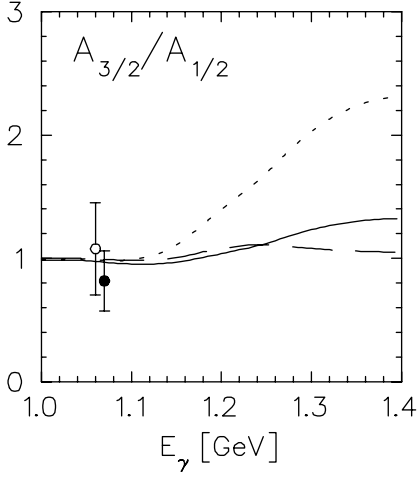


FIG. 6: Ratio $A_{3/2}/A_{1/2}$ of the helicity amplitudes for $D_{33}(1700)$ as a function of the lab photon energy. The solid, dashed, and dotted curves correspond to the solutions I, II, and III from Table II. The empty circle shows the ratio obtained in ref. [11], whereas the filled circle is the value advocated by PDG [10].

addition of the nonzero $D_{33} \rightarrow \pi N^*$ coupling results in an approximately linear dependence on $\cos \theta_{\pi}^H$ (there is an additional dependence of the factors $F^{D_{33}(\pi N^*)}$ and X_{π} in (22) on $\cos \theta_{\pi}^H$, which is, however, rather weak). The corresponding coefficient B is proportional to $Re(\bar{c}_1 c_2)$ (24) and is therefore rather sensitive even to a small admixture of πN^* .

In the canonical frame one has

$$\begin{aligned} \frac{d\sigma}{d\omega_{\pi N} d\Omega_{\pi}^K d\cos \Theta_{\eta}} \sim \\ A_{1/2}^2 \left(|c_1|^2 + |c_2|^2 - 2Re(\bar{c}_1 c_2) \cos \theta_{\pi\eta} \right) \\ + \left(A_{3/2}^2 - A_{1/2}^2 \right) \left(|c_1|^2 \sin^2 \theta_{\pi}^K + |c_2|^2 \sin^2 \Theta_{\eta} \right. \\ \left. + 2Re(\bar{c}_1 c_2) \sin \theta_{\pi}^K \sin \Theta_{\eta} \cos \phi_{\pi}^K \right), \end{aligned} \quad (31)$$

with $\theta_{\pi\eta}$ being the angle between \vec{q}_{π}^* and \vec{q}_{η} . Although the formula (31) looks less cumbersome than eq. (21), the coefficients c_1 and c_2 are now functions of all four variables $\omega_{\pi N}$, Ω_{π}^K , and $\cos \Theta_{\eta}$. Therefore, a simple general analysis, like in the case of the H system, is not possible. The only conclusion we can draw is that since c_1 and c_2 depend rather weakly on the angle ϕ_{π}^K , the distribution $W(\phi_{\pi}^K)$ can approximately be represented in the form

$$W(\phi_{\pi}^K) \approx \frac{1}{2\pi} \left(1 + \frac{1-a}{1+a} \tilde{C} \cos \phi_{\pi}^K \right), \quad (32)$$

where the coefficient \tilde{C} is equal to

$$\begin{aligned} \tilde{C} = \frac{2}{N} \int Re(\bar{c}_1 c_2) \\ \times \sin \Theta_{\eta} \sin \theta_{\pi}^K d\omega_{\pi N} d\cos \Theta_{\eta} d\cos \theta_{\pi}^K. \end{aligned} \quad (33)$$

A look at eqs. (33) and (27) shows that, contrary to $W(\phi_{\pi}^H)$ whose form depends only on the parameter a , in the K frame the ϕ_{π}^K -dependence is solely due to interference between $\eta\Delta$ and πN^* mechanisms. We therefore expect that the shape of $W(\phi_{\pi}^K)$ is much more sensitive to the πN^* contribution than the ϕ_{π} -distribution in the helicity system. This assumption is well confirmed by the analysis of ref. [8].

In Fig. 5 we demonstrate our results for different angular distributions. As noted above, we choose as independent kinematic variables those associated with the $\eta + (\pi N)$ partition. Namely, the results are presented for the distributions $W(\theta_{\pi}^{K(H)})$ and $W(\phi_{\pi}^{K(H)})$ over the pion angle in the K and H system (see Fig. 2), as well as for the distribution $W(\Theta_{\eta})$ over the angle of the η momentum in the overall c.m. frame. The solid, long-dashed, and dotted curves present three different solutions, providing an acceptable description of the data. The resulting parameter sets corresponding to each solution are collected in Table II. The partial cross sections in the last column in this Table are calculated according to formula (20) at the energy $W = M_R$, and give approximate contributions of the corresponding resonances to the total cross section.

It is worth mentioning that the fits collected in Table II do not necessarily give the lowest value of χ^2 . Rather, we present them as three sample results which describe the same data via different dynamical contents. Namely, solution I (first row in Table II, solid line in Fig. 5) is mostly consistent with our assumption about D_{33} dominance over the whole energy region considered. Here other partial waves are of relatively minor importance. Solution II (second row, long-dashed line in Fig. 5) describes the data at $E_{\gamma} > 1.2$ GeV via an appreciably large contribution of the resonance $P_{33}(1920)$. Finally, solution III (third row, dotted curve in Fig. 5) contains a small admixture of the d -wave in $D_{33}(1700) \rightarrow \eta\Delta$ decay, which is neglected in the first two cases.

The following conclusions can be drawn:

(i) The general properties of the data in Fig. 5 (the number of minima and the convexity direction) are roughly described with only the D_{33} wave. This fact, considered as a strong evidence of the D_{33} dominance was already discussed in ref. [8]. In particular, one can see that at energies above $E_{\gamma} = 1.2$ GeV the experimentally observed shape of $W(\theta_{\pi}^H)$ and $W(\phi_{\pi}^H)$ is rather close to the predicted form $a + b \cos \theta_{\pi}^H$ and $c + d \cos 2\phi_{\pi}^H$ (eqs. (24) and (27)). In the canonical frame the distribution $W(\phi_{\pi}^K)$ is also in good agreement with the analytic form $A + B \cos \phi_{\pi}^K$ provided by the single D_{33} model (see eq. (32)). As is shown in ref. [8], other partial waves fail to describe all the angular distributions simultaneously.

(ii) Since the coefficient C in eq. (27) is a constant, the ϕ_{π}^H dependence is totally determined by $\cos 2\phi_{\pi}^H$. Then, the convexity direction of $W(\phi_{\pi}^H)$ (up or down) is governed by the sign of the difference $1 - a$. Therefore, the observed ϕ_{π}^H -dependence allows one to make a conclusion about the value of the parameter a . More specifically, ac-

TABLE II: Parameters of the isobar model fitted to the data in Fig. 5. The first three rows give the parameter sets, to which we refer in the text as solutions I, II, and III. The forth row lists the corresponding numbers given by the Particle Data Group [10]. The sign of $\sqrt{\beta_{\eta\Delta}}A_{1/2}$ is the sign of the product of $A_{1/2}$ and the $R \rightarrow \eta\Delta$ coupling constant $f_{R\Delta\eta}$ (see eq. (12)). The relative sign between $R \rightarrow \eta\Delta$ and $R \rightarrow \pi N^*$ couplings is taken positive for all resonances. The partial cross sections σ^R are calculated according to the approximate formula (20) at $W = M_R$. An extremely large (small) value of the ratio r (see, e.g., those for $P_{31}(1750)$ and $F_{35}(1905)$) means that the corresponding partial decay width $\Gamma_{\pi\eta N}^{(\eta\Delta)}$ ($\Gamma_{\pi\eta N}^{(\pi N^*)}$) is close to zero. $\chi^2/N = 2.76, 3.06$, and 3.39 for the solutions I, II, and III, respectively.

| $J^\pi[L_{2T2J}(M_R)]$ | M_R | $\Gamma_{tot}^R(M_R)$ | $\sqrt{\beta_{\eta\Delta}}A_{1/2}(M_R)$ | $\frac{A_{3/2}(M_R)}{A_{1/2}(M_R)}$ | $r = \frac{\Gamma_{\pi\eta N}^{(\pi N^*)}(M_R)}{\Gamma_{\pi\eta N}^{(\eta\Delta)}(M_R)}$ | $\sigma^R(M_R)$ |
|--------------------------------|--------------|-----------------------|---|-------------------------------------|--|----------------------|
| | [MeV] | [MeV] | $[10^{-3}\text{GeV}^{-1/2}]$ | | | $[\mu\text{b}]$ |
| $\frac{3}{2}^- [D_{33}(1700)]$ | 1701 ± 1 | 375 | 10.6 ± 0.2 | 0.95 ± 0.01 | 0.70 ± 0.03 | 0.186 |
| | 1720 | 375 | 15.1 | 0.95 | 0.67 | 0.384 |
| | 1709 | 375 | 14.8 | 1.00 | 0.67 | 0.370 |
| | 1700 | 300 | | 0.82 | | |
| $\frac{3}{2}^+ [P_{33}(1600)]$ | 1657 ± 5 | 350 | -0.10 ± 0.011 | 0.39 ± 0.06 | 1.78 ± 0.32 | $6.70 \cdot 10^{-6}$ |
| | 1636 | 350 | 0.17 | 1.20 | 169 | $7.02 \cdot 10^{-3}$ |
| | 1670 | 350 | 0.18 | 3.71 | 71.4 | $1.90 \cdot 10^{-2}$ |
| | 1600 | 350 | | 0.39 | | |
| $\frac{1}{2}^+ [P_{31}(1750)]$ | 1832 ± 1 | 400 | 8.35 ± 0.9 | | 0.22 ± 0.11 | $3.78 \cdot 10^{-2}$ |
| | 1820 | 400 | 9.93 | | $2.6 \cdot 10^{-2}$ | $4.53 \cdot 10^{-2}$ |
| | 1826 | 400 | 40.2 | | $1.0 \cdot 10^{-3}$ | 0.720 |
| | 1750 | | | | | |
| $\frac{5}{2}^+ [F_{35}(1905)]$ | 1873 ± 4 | 330 | -25.5 ± 0.6 | -0.70 ± 0.03 | $(9.1 \pm 7.5) \cdot 10^{-3}$ | 0.506 |
| | 1890 | 330 | -10.8 | -1.64 | $1.7 \cdot 10^{-2}$ | 0.231 |
| | 1890 | 330 | $9.3 \cdot 10^{-4}$ | -1.94 | $1.1 \cdot 10^6$ | $2.38 \cdot 10^{-3}$ |
| | 1890 | 330 | | -1.73 | | |
| $\frac{3}{2}^+ [P_{33}(1920)]$ | 1894 ± 3 | 200 | 11.87 ± 0.42 | 1.15 ± 0.06 | 0.14 ± 0.09 | 0.319 |
| | 1842 | 200 | 15.5 | 1.49 | 0.89 | 1.29 |
| | 1848 | 200 | 4.42 | 1.62 | 6.4 | 0.462 |
| | 1920 | 200 | | 0.575 | | |
| $\frac{3}{2}^- [D_{33}(1940)]$ | 1870 ± 1 | 450 | 19.9 ± 1.1 | 1.65 ± 0.02 | 0.22 ± 0.03 | 0.695 |
| | 2069 | 450 | -37.6 | 1.77 | 0.10 | 2.26 |
| | 1937 | 450 | $-7.8 \cdot 10^{-3}$ | 5.09 | $1.1 \cdot 10^6$ | 1.04 |
| | 1940 | | | | | |

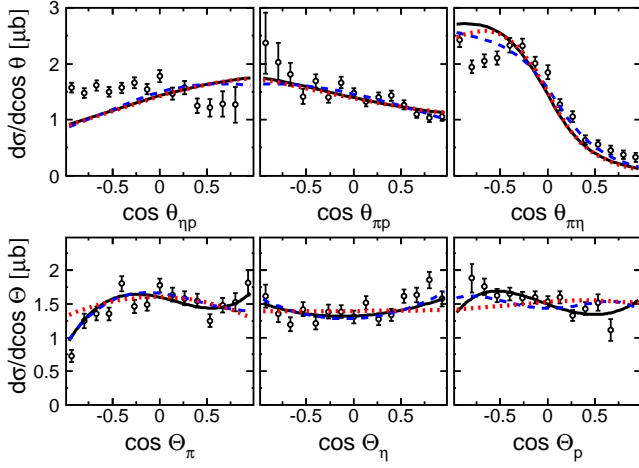


FIG. 7: Our prediction of angular distributions for energy bin $1.7 < W < 1.9$ GeV compared with the CB-ELSA data of ref. [3] (open circles). In the first row, the angle θ_{ij} is the angle of the i th particle in the ij c.m. frame with respect to the momentum of the third particle. In the second row, Θ is the angle of the corresponding particle in the overall c.m. frame. The solid (dashed) curve is obtained with the parameter set I (II) from Table II. The dotted curve includes only the D_{33} wave. The theoretical results have arbitrary normalization.

cording to the expression (27), the characteristic shape of $W(\phi_\pi^H)$ with the minima at $\phi_\pi^H = \pi/2$ and $\phi_\pi^H = 3\pi/2$, visible at $E_\gamma > 1.2$ GeV, should point to the fact that at this energy $a > 1$ (eq. (27)). This result is also confirmed by $W(\theta_\pi^K)$ (first row in Fig. 5) which, as follows from (32) and (33), would otherwise be convex down in contrast to the data.

Our results for the ratio $A_{3/2}/A_{1/2}$, as a function of the photon energy, are presented in Fig. 6. As may be seen, version III requires an unexpectedly sharp energy dependence of this parameter, so that already at $E_\gamma = 1.4$ GeV it amounts up to 2.4, thus visibly exceeding the average PDG value 0.817 ± 0.242 . At the same time, versions I and II allow one to suppress the undesirable increase of this ratio at higher energies.

(iii) According to our qualitative discussion above (see text after eq. (30)), the visible forward-backward asymmetry in $W(\theta_\pi^H)$ may be interpreted as a signal of a nonzero πN^* contribution. This conclusion is trivial in the sense that the πN^* channel always contributes to the reaction $\gamma p \rightarrow \pi^0 \eta p$ via ηp interaction in the final state. However as noted in the Introduction, direct measurement of the ηp spectrum to study the role of this channel may fail, primarily because of the overwhelming contribution of the $\eta \Delta$ decay mode. At the same time, the role of πN^* may be estimated rather precisely using the asymmetry rate of $W(\theta_\pi^H)$. Indeed, as is shown in [6], here the different states J^π are added incoherently, so that the shape of $W(\theta_\pi^H)$ is always symmetric if only the channel $\eta \Delta$ is taken into account. In this respect,

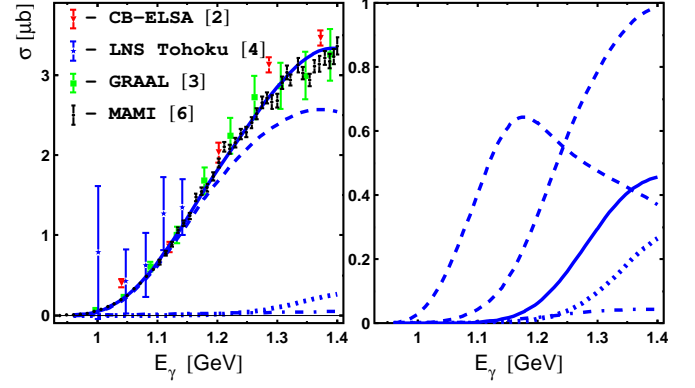


FIG. 8: Total cross sections for $\gamma p \rightarrow \eta \pi^0 p$. The theoretical results are obtained with parameter set I in Table II. Left panel: full calculation (solid curve), D_{33} wave (dashed curve), P_{33} wave (dotted curve), Born terms, shown by the diagrams (a)-(f) in Fig. 1, (dash-dotted curve). Right panel: the contribution of $D_{33}(1700)$ and $D_{33}(1940)$ (dashed curves), $F_{35}(1905)$ (solid), $P_{33}(1920)$ (dotted), $P_{31}(1750)$ (dash-dotted).

the observed asymmetry is a direct consequence of the interference between $\eta \Delta$ and πN^* mechanisms.

(iv) In the region $E_\gamma = 1.2 - 1.4$ GeV, the distribution $W(\Theta_\eta)$ over the η angle in the overall c.m. system demonstrates the characteristic shape $a + b \cos^2 \Theta$, vanishing at lower energies. This feature is explained in different ways in our fits I-III. For example, the parameter sets I and II describe $W(\Theta_\eta)$ via a relatively strong contribution of $F_{35}(1905)$ and $P_{33}(1920)$ respectively. In the third version of the model, the increasing role of the $\cos^2 \Theta$ term is ascribed to the d -wave fraction in the $\eta \Delta$ decay of $D_{33}(1700)$. Since the D_{33} mass is pretty close to the $\pi \eta$ threshold, even a small d -wave admixture in the $\eta \Delta$ mode may lead to a sizable contribution of this wave at energies above $E_\gamma = 1.2$ MeV. The dotted curve in Fig. 5 is obtained by assuming that the d -wave fraction comprises only 2% of the total $D_{33} \rightarrow \pi \eta N$ width.

(v) In Fig. 7 we show our prediction of some angular distributions for three different partitions, $\pi^0 + (\eta p)$, $\eta + (\pi^0 p)$, and $p + (\pi^0 \eta)$, together with the data obtained in ref. [3]. As one can see, our calculations are in general agreement with the experimental results, perhaps except for the distribution over $\cos \theta_{\eta p}$. At the same time, these observables demonstrate a rather weak sensitivity to the model ingredients. Already the single D_{33} model (short-dashed line in Fig. 7) correctly predicts the main features of all distributions. Addition of other resonances does not visibly change the calculation. On the whole, all three parameter sets in Table II give equally good descriptions of the data.

(vi) As noted in the Introduction, the D_{33} wave seems to also remain important at higher energies. We base this conclusion on the fact that the single D_{33} model works quite well at $E_\gamma > 1.3$ GeV (short-dashed line in

Fig. 5). At the same time, our prediction for the total cross section with only $D_{33}(1700)$ starts to already underestimate the data at $E_\gamma = 1.1$ GeV. This may be considered as an indication of an additional source of the D_{33} wave which should come into play at higher energies. In ref. [3] this effect is ascribed to $D_{33}(1940)$ which is classified as a one-star resonance in the PDG listing [10]. In the present work, to maintain the growth of the partial cross section $\sigma^{D_{33}}$ we also introduce this resonance with free parameters. However, one has to keep in mind that since $D_{33}(1940)$ is at the upper limit of our energy region, the fitting results are not very sensitive to the exact contribution of this resonance. The same must hold true for $P_{33}(1920)$.

(vii) Fig. 8 demonstrates our calculation of the total cross section, where contributions of individual terms entering the amplitude are plotted separately. The results are obtained with the parameter set corresponding to the solution I in Table II. We prefer this version of our model since, as will be shown in the next section, it also yields a reasonable description of the beam asymmetry, in contrast to the solutions II and III. The reader should not be surprised by the quality of our description in Fig. 8 since, as noted in Sect. II, the total cross section was effectively included into the fit (see the comment after eq. (15)).

As predicted by solution I, the major fraction of the reaction yield is provided by the coherent sum of the resonances $D_{33}(1700)$ and $D_{33}(1940)$ (short-dashed line on the left panel in Fig. 8). The contribution of $D_{33}(1940)$ is comparable to that of $D_{33}(1700)$. As pointed out above, the need for the former resonance in our calculation is mainly dictated by the necessity to prevent the D_{33} wave from dying out when $D_{33}(1700)$ rapidly falls-off above $E_\gamma > 1.2$ GeV. Otherwise the model leaves room for $P_{33}(1920)$ leading to solution II. As follows from Table II, in this case the contribution of $P_{33}(1920)$ amounts up to 40 % of the total cross section at $E_\gamma = 1.4$ GeV.

It is quite remarkable that the role of $P_{33}(1600)$ in our analysis turns out to be insignificant. The reason is that in the near-threshold region some fraction of the p -wave comes from the background. The corresponding p -wave admixture turns out to be sufficient to obtain a more or less accurate description of the forward-backward asymmetry in the angular distribution $W(\Theta_\eta)$ of η mesons in the overall c.m. system. At the same time, at higher energies, where the role of D_{33} strongly increases, the background is unable to give the necessary p -wave fraction. As a result, our fit requires inclusion of other resonances with positive parity, in particular $P_{31}(1750)$, $F_{35}(1905)$, as well as $P_{33}(1920)$.

B. Beam asymmetry

The beam asymmetry Σ for linearly polarized photons has been measured in refs. [4] and [13]. It was presented as a function of the invariant mass of three two-particle subsystems $\pi^0 p$, ηp , and $\pi^0 \eta$. In the region $E_\gamma < 1.5$ GeV

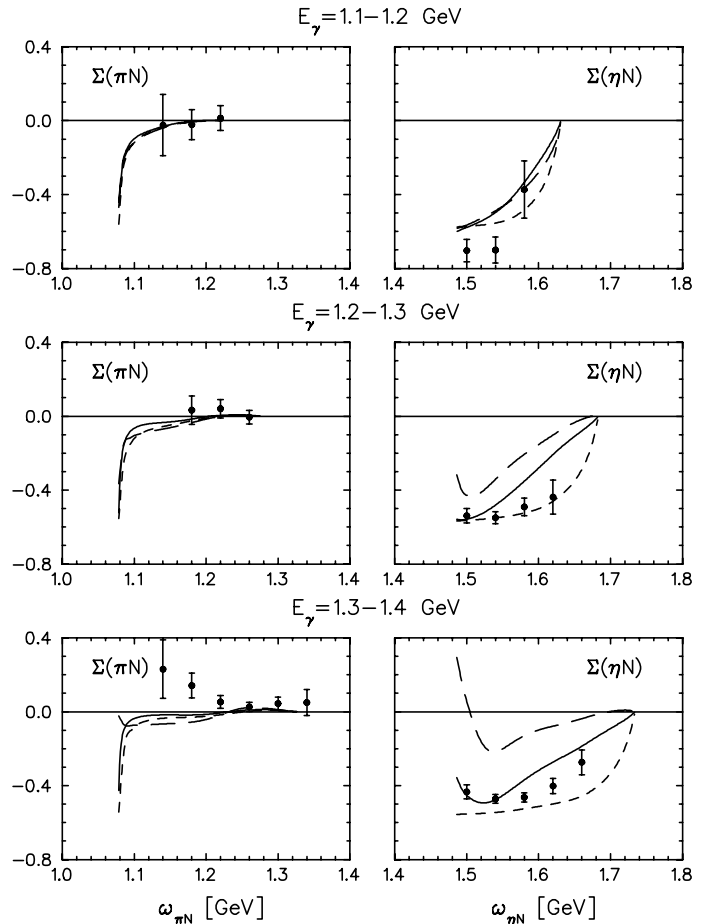


FIG. 9: Beam asymmetry for $\gamma p \rightarrow \pi^0 \eta p$ averaged over three intervals of the beam energy. The data are from ref. [4]. The solid (long-dashed) curve is our prediction corresponding to the parameter set I (II) in Table II. The short-dashed curve includes only the D_{33} wave.

this observable demonstrates several properties, which we would like to discuss. Firstly, the data show (see Figs. 9 and 10) that in the $\pi^0 p$ case, when the reaction plane is fixed by the condition $\phi_\eta = 0$ in the overall c.m. system, the value of Σ (hereafter denoted by $\Sigma(\pi N)$) is comparable to zero in almost the whole region of $\omega_{\pi N}$, except for the lower boundary of the spectrum. In the channel ηp , where $\phi_\pi = 0$, the beam asymmetry $\Sigma(\eta N)$ is negative and its absolute value comprises about 0.5.

Both features may be qualitatively explained by the dominance of the D_{33} partial wave. Indeed, keeping only D_{33} in the sum (4), for the polarized cross section one ob-

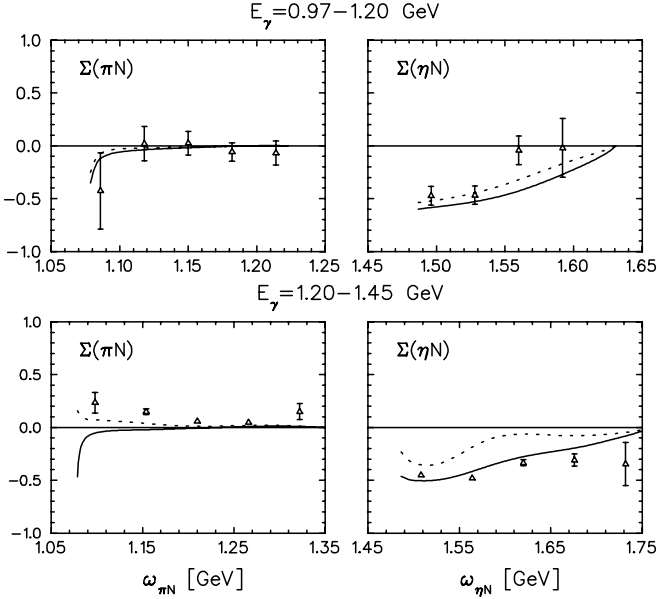


FIG. 10: Same as in Fig. 9 but for other energy bins. The data are taken from ref. [13]. The solid (dotted) curve corresponds to the solution I (III) in Table II.

tains (omitting unessential angular independent factors)

$$\begin{aligned} \Sigma \frac{d\sigma}{d\omega_{\pi p}} &= \frac{1}{2} \left(\frac{d\sigma_{\perp}}{d\omega_{\pi p}} - \frac{d\sigma_{\parallel}}{d\omega_{\pi p}} \right) \\ &\sim -\frac{A_{1/2}A_{3/2}}{\sqrt{3}} \int_0^{\pi} \sin \theta_{\pi}^H d\theta_{\pi}^H \\ &\times \left(|c_1|^2 \frac{1}{2} (3 \cos^2 \theta_{\pi}^H - 1) + |c_2|^2 \right. \\ &\left. + 2\Re(\bar{c}_1 c_2) \cos \theta_{\pi}^H \right), \end{aligned} \quad (34)$$

where the coefficients c_i are determined in eqs. (22) and (23). In eq. (34) σ_{\perp} (σ_{\parallel}) is the cross-section with the photon beam polarized perpendicular (parallel) to the reaction plane. The corresponding unpolarized cross section reads

$$\begin{aligned} \frac{d\sigma}{d\omega_{\pi p}} &= \frac{1}{2} \left(\frac{d\sigma_{\perp}}{d\omega_{\pi p}} + \frac{d\sigma_{\parallel}}{d\omega_{\pi p}} \right) \\ &\sim \frac{1}{2} \left(A_{1/2}^2 + A_{3/2}^2 \right) \int_0^{\pi} \sin \theta_{\pi}^H d\theta_{\pi}^H \\ &\times \left(|c_1|^2 + |c_2|^2 + 2\Re(\bar{c}_1 c_2) \cos \theta_{\pi}^H \right). \end{aligned} \quad (35)$$

It is now straightforward to obtain an analytic expression for the beam asymmetry dividing eq. (34) by eq. (35).

In the partition $\pi + (\eta N)$ the expressions for $\Sigma \frac{d\sigma}{d\omega_{\eta N}}$ and for the unpolarized cross section $\frac{d\sigma}{d\omega_{\eta N}}$ are formally

identical to that given by (34) and (35)

$$\begin{aligned} \Sigma \frac{d\sigma}{d\omega_{\eta p}} &\sim -\frac{A_{1/2}A_{3/2}}{\sqrt{3}} \int_0^{\pi} \sin \theta_{\eta}^H d\theta_{\eta}^H \\ &\times \left(|b_1|^2 \frac{1}{2} (3 \cos^2 \theta_{\eta}^H - 1) + |b_2|^2 \right. \\ &\left. + 2\Re(\bar{b}_1 b_2) \cos \theta_{\eta}^H \right), \end{aligned} \quad (36)$$

$$\begin{aligned} \frac{d\sigma}{d\omega_{\eta p}} &\sim \frac{1}{2} \left(A_{1/2}^2 + A_{3/2}^2 \right) \int_0^{\pi} \sin \theta_{\eta}^H d\theta_{\eta}^H \\ &\times \left(|b_1|^2 + |b_2|^2 + 2\Re(\bar{b}_1 b_2) \cos \theta_{\eta}^H \right), \end{aligned} \quad (37)$$

except that the integration variable is now θ_{η}^H and the coefficients c_i are replaced by b_i , determined as

$$b_1 = -F^{D_{33}(\eta\Delta)} X_{\pi} q_{\eta}^*, \quad (38)$$

$$b_2 = \left(F^{D_{33}(\eta\Delta)} (1 - X_{\pi} X_{\eta}) + F^{D_{33}(\pi N^*)} \right) q_{\pi}. \quad (39)$$

With increasing ω_{α} , the value of $\Sigma(\pi N)$ rapidly goes to zero, whereas $\Sigma(\eta N)$ demonstrates a rather smooth dependence. This qualitative difference may be explained by the kinematic effect caused by the rather large mass difference of the π and η mesons.

Indeed, because of the small mass of the pion, its momentum in the major part of the reaction phase space is essentially higher than the η momentum. As a consequence, in the partition $\eta + (\pi N)$ we will have (see eqs. (22) and (23))

$$\left| \frac{c_1}{c_2} \right|^2 \sim \left(\frac{q_{\pi}^*}{q_{\eta}} \right)^2 \gg 1. \quad (40)$$

For example, taking for the parameter r the value $r = 0.7$, as predicted by the fit I, we will have $|c_1/c_2|^2 \approx 27$ at $W = 1.7$ GeV, which further increases to 74 at $W = 1.9$ GeV.

Since in the cross sections (34) and (35) the coefficients c_i appear in the integrand, it is more appropriate to compare directly the corresponding integrated values. As an example, in Fig. 11 we show the integrals

$$I_i = \int_0^{\pi} |c_i|^2 \sin \theta_{\pi}^H d\theta_{\pi}^H, \quad i = 1, 2, \quad (41)$$

$$J_i = \int_0^{\pi} |b_i|^2 \sin \theta_{\eta}^H d\theta_{\eta}^H, \quad i = 1, 2, \quad (42)$$

calculated at $E_{\gamma} = 1.2$ GeV, as functions of the energy ω_{α} , $\alpha = \eta\Delta, \pi N^*$. As noted above, in the region of very low $\omega_{\pi N}$ where $q_{\pi}^* \simeq 0$ we have $I_1 \ll I_2$. However, with increasing $\omega_{\pi N}$ the pion momentum q_{π}^* rapidly increases, so that the relation $I_1 \gg I_2$ holds in almost the whole

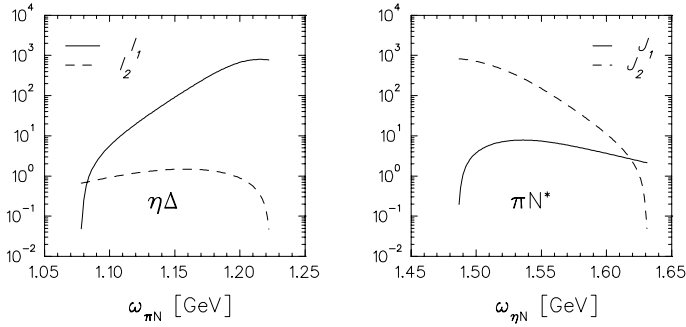


FIG. 11: Integrals (41) and (42) calculated at photon energy $E_\gamma=1.2$ GeV. The values are given in arbitrary units.

region of $\omega_{\pi N}$. For instance, as may be seen from Fig. 11, already at $\omega_{\pi N} = 1.15$ GeV we have $I_1/I_2 \simeq 10^2$.

At the same time, in the polarized cross section $\Sigma \frac{d\sigma}{d\omega_{\pi N}}$ the coefficient $|c_1|^2$ enters with the weight $P_2(\cos\theta_\pi^H) = (3\cos^2\theta_\pi^H - 1)/2$ (see eq. (34)), which strongly reduces its contribution after integration over θ_π^H . This last effect is due to the rather smooth dependence of $|c_1|^2$ on $\cos\theta_\pi^H$. As a consequence, the value of $\Sigma(\pi N)$ turns out to be roughly equal to

$$\Sigma(\pi N) \simeq \frac{I_2}{I_1 + I_2} \simeq \frac{I_2}{I_1} \ll 1. \quad (43)$$

In other words, in the region where the D_{33} wave dominates, the nonzero value of the asymmetry $\Sigma(\pi N)$ is due to the nontrivial contribution of the πN^* configuration to the D_{33} decay. For this reason, the rapid decrease of $\Sigma(\pi N)$ at moderate $\omega_{\pi N}$ is due to the decrease of this contribution to the integral in eq. (34). The latter has a kinematic reason and, as we have just explained, is eventually caused by the mass difference between π and η mesons.

In the second case, when the reaction plane is fixed by $\phi_\eta = 0$ (partition $\eta + (\pi N)$), the situation is just the opposite. Namely, (see eqs. (38)-(39))

$$\left| \frac{b_1}{b_2} \right|^2 \sim \left(\frac{q_\eta^*}{q_\pi} \right)^2 \ll 1, \quad (44)$$

so that

$$|\Sigma(\eta N)| \simeq \left| \frac{J_2}{J_1 + J_2} \right| \simeq 1. \quad (45)$$

In the same limiting case $\omega_{\eta N} \rightarrow 0$ ($b_1 \rightarrow 0$), we get from eqs. (36) and (37) a simple relation between the parameter a (29) and the value of $\Sigma(\eta N)$

$$\Sigma(\eta N) = -\frac{2}{\sqrt{3}} \frac{\sqrt{a}}{1+a}. \quad (46)$$

Taking $a = 1.2$ (the average of this parameter in the region $E_\gamma = 1.0 - 1.4$ GeV) we will have $\Sigma(\eta N) = -0.43$,

which is consistent with the experimental result. Since $|\Sigma(\eta N)|$ (46) has maximum $|\Sigma(\eta N)| = 1/\sqrt{3}$ at $a = 1$, it appears to be rather insensitive to a as long as a does not strongly differ from unity.

In a similar manner, at $\omega_{\pi N} \rightarrow 0$ we have $c_1 \sim q_\pi^* \rightarrow 0$ and the value of $\Sigma(\pi N)$ depends only on the parameter a (29). As a result, in the single D_{33} model (or generally in the single resonance model) one has the simple relation

$$\Sigma(\pi N) \Big|_{\omega_{\pi N} \rightarrow 0} = \Sigma(\eta N) \Big|_{\omega_{\eta N} \rightarrow 0}. \quad (47)$$

It is also worth noting that, according to the formula (36), the negative value of the asymmetry $\Sigma(\eta N)$ is a signature of the fact that $A_{1/2}^{D_{33}}$ and $A_{3/2}^{D_{33}}$ should have the same sign.

Our results for the photon asymmetry predicted by the three solutions discussed in the previous section are presented in Figs. 9 and 10. As we can see, only version I of our model where the D_{33} wave dominates in the whole energy region is able to reproduce the main features of the measured asymmetry. As would be expected, the predicted behavior is close to that given by the single D_{33} model, so that inclusion of other resonances does not give rise to a crucial change. At the same time, version II containing an appreciable contribution of $P_{33}(1920)$ (see the last column in Table II) yields a rather poor description of $\Sigma(\eta N)$ in the region $1.3 \leq E_\gamma \leq 1.4$ GeV. As one can see from Fig. 9, at low invariant energies $\omega_{\eta N}$ this resonance causes an undesirable shift to positive values, in contrast to the data demonstrating a rather smooth dependence on $\omega_{\eta N}$.

IV. CONCLUSION

We performed a phenomenological analysis of the photon-induced $\pi^0\eta$ production at energies within the region $1.0 \leq E_\gamma \leq 1.4$ GeV. The data contain detailed information on angular distributions to determine, at least qualitatively, the angular momentum content of the reaction amplitude.

As is repeatedly mentioned in the paper, among different mechanisms which might contribute to the reaction, the excitation of the D_{33} wave turns out to be most evident in the data. According to our calculation, at the lab photon energy $E_\gamma = 1.1$ GeV and above the coherent sum of $D_{33}(1700)$ and $D_{33}(1940)$ can account for the majority of the experimental results. We pay some attention to a qualitative discussion of the way in which the main features of the angular distributions determine some of the adjustable parameters of the model.

At the same time, deviations from the single D_{33} model predictions point to a nontrivial admixture of other resonance states. That these 'weaker' resonances should have positive parity is confirmed by visible forward-backward asymmetry in the $\cos\Theta_\eta$ distribution in the overall c.m. frame (fifth column in Fig. 5). Inclusion of $P_{33}(1600)$,

$P_{31}(1750)$, and $F_{35}(1905)$, improves the quality of our fit.

Furthermore, in order to maintain the rather monotone rise demonstrated by the measured total cross section up to $E_\gamma = 1.4$ GeV we are forced to include the tails of the resonance states with higher masses. Taking into account the results obtained in ref. [3], the resonance $P_{33}(1920)$ as well as the one-star resonance $D_{33}(1940)$ were included into the model. We allow their parameters to be varied, although the energy region covered by the measurements does not permit an unambiguous determination of their values.

On the whole, our results, at least those corresponding to solution I, are rather close to the results obtained in ref. [3]. We also see that a more rigorous study of the partial wave structure of $\pi^0\eta$ photoproduction requires detailed polarization data. Otherwise, the theory admits a variation of the resonance parameters over a relatively wide range. As an example, we give three versions of the fit which explain the features of the observables via different mechanisms. In particular, the characteristic shape of $W(\Theta_\eta)$ at higher energies, with a minimum at $\cos\Theta_\eta = 0$, may be described via different dynamical contents. In version III this shape is reproduced if we allow for a small admixture of the d -wave mode in the $\eta\Delta$ decay of the $D_{33}(1700)$. In the other two cases the same effect was provided by the contribution of P_{33} and/or F_{35} states.

We also explored in considerable detail the photon

asymmetry Σ , and found that its main features may well be interpreted in terms of the single D_{33} model. In this model the nontrivial value of $\Sigma(\pi N)$ is a simple consequence of $\eta\pi$ interaction in the final state. Inclusion of other resonances leads to rather small corrections. However, as pointed out in Sect. III B, the behavior of $\Sigma(\eta N)$ in the region of low ηN invariant energies is quite sensitive to the contribution of the P_{33} wave. In particular, our solution II containing a large contribution of $P_{33}(1920)$ turns out to be inconsistent with the available data for $\Sigma(\eta N)$.

Further study of the reaction $\gamma p \rightarrow \pi^0\eta p$ may be aimed at those observables, in which the contributions of positive parity resonances may be identified in a model independent way, wherever possible. With new data for polarization observables one may expect considerable improvement of accuracy in the determination of the resonance parameters. In the past year some progress has been made towards that goal in refs. [15] and [16].

This work was supported by the Deutsche Forschungsgemeinschaft (SFB 443), DFG-RFBR (Grant No. 09-02-91330), the European Community-Research Infrastructure Activity under the FP6 “Structuring the European Research Area” programme (Hadron Physics, contract number RII3-CT-2004-506078), and the RF Presidential Grant (No MD-2772.2007.2). A. Fix would like to thank the Institut für Kernphysik of the Johannes Gutenberg-Universität Mainz for the kind hospitality.

-
- [1] M. Döring, E. Oset, and D. Strottman, Phys. Rev. C **73**, 045209 (2006).
 - [2] M. Döring, E. Oset, and D. Strottman, Phys. Lett. B **639**, 59 (2006); Acta Phys. Slov. **56** (2006) 221
 - [3] I. Horn *et al.*, Eur. Phys. J. A **38**, 173 (2008).
 - [4] J. Ajaka *et al.*, Phys. Rev. Lett. C **100**, 052003 (2008).
 - [5] T. Nakabayashi *et al.*, Phys. Rev. C **74**, 035202 (2006).
 - [6] A. Fix, M. Ostrick, and L. Tiator, Eur. Phys. J. A **36**, 61 (2008), DOI: 10.1140/epja/i2007-10551-x.
 - [7] S. Sarkar, E. Oset, and M. J. Vicente Vacas, Nucl. Phys. A **750**, 294 (2005).
 - [8] V. L. Kashevarov, A. Fix *et al.*, Eur. Phys. J. A **42**, 141 (2009), DOI: 10.1140/epja/i2009-10868-4.
 - [9] A. V. Anisovich *et al.*, J. Phys. G **28**, 15 (2002).
 - [10] C. Amsler *et al.*, [Particle Data Group], Phys. Lett. **B667**, 1 (2008).
 - [11] R. A. Arndt, W. J. Briscoe, I. I. Strakovsky, and R. L. Workman, Phys. Rev. C **74**, 045205 (2006).
 - [12] D. M. Manley and E. M. Saleski, Phys. Rev. D **45**, 4002 (1992).
 - [13] E. Gutz, V. Sokhoyan, H. van Pee *et al.*, Eur. Phys. J. A **35**, 291 (2008).
 - [14] S. Capstick and C. Isgur, Phys. Rev. D **34**, 2809 (1986); S. Capstick and W. Roberts, Phys. Rev. D **49**, 4570 (1994).
 - [15] E. Gutz, V. Sokhoyan, H. van Pee *et al.*, Phys. Lett. B **687**, 11 (2010).
 - [16] M. Döring, E. Oset, and Ulf-G. Meissner, e-Print: arXiv:1003.0097 [nucl-th].